



McMillan, M. D., Booker, J. D., Smith, D. J., Onisa, C. F., Korsunsky, A. M., Song, X., ... Evans, A. (2016). Analysis of increasing torque with recurrent slip in interference-fits. *Engineering Failure Analysis*, 62, 58-74. DOI: 10.1016/j.engfailanal.2015.12.005

Peer reviewed version

Link to published version (if available):  
[10.1016/j.engfailanal.2015.12.005](https://doi.org/10.1016/j.engfailanal.2015.12.005)

[Link to publication record in Explore Bristol Research](#)  
PDF-document

## **University of Bristol - Explore Bristol Research**

### **General rights**

This document is made available in accordance with publisher policies. Please cite only the published version using the reference above. Full terms of use are available:  
<http://www.bristol.ac.uk/pure/about/ebr-terms.html>

# ANALYSIS OF INCREASING TORQUE WITH RECURRENT SLIP IN INTERFERENCE-FITS

MD McMillan<sup>1</sup>, JD Booker<sup>1</sup>, DJ Smith<sup>1</sup>, C Fedorciuc Onisa<sup>2</sup>, AM Korsunsky<sup>3</sup>, X Song<sup>3</sup>, N Baimpas<sup>3</sup>, A Evans<sup>4</sup>.

<sup>1</sup> Department of Mechanical Engineering, University of Bristol, UK.

<sup>2</sup> TATA Steel, Swindon RD&T, Rotherham, UK.

<sup>3</sup> Department of Engineering Science, University of Oxford, UK

<sup>4</sup> SALSA, ILL, Grenoble, France

## Abstract

*Previous research associated with interference-fitted assemblies has shown that as recurring slip occurs (i.e. load to total slip, unloading and reload to total slip) there is an observed increase in the holding torque after each loading cycle. The aim of this work was to identify the reasons for this 'torque strengthening' phenomenon. The work also has industrial relevance in the optimum design of interference-fitted rolls used for the hot rolling of steel sections. Previous work has shown that the major contributors to the overall holding torque were the interface pressure, material properties and the coefficient of friction between component materials. In this work, neutron diffraction tests and crack compliance tests showed no correlation between the interface pressure and increased holding torque. Meanwhile, experimental holding torque tests on sample interference-fits showed that for each recurring holding torque failure (slip) in a test cycle, the holding torque increased. Subsequent wear investigations showed that the wear of the surfaces increased throughout the testing and once a specific type of wear had occurred through a 'ploughing' mechanism, significant damage could be done to the more expensive shaft component. These observations suggest that an effective increase in the coefficient of friction between shaft and hub is responsible for the increase in holding torque, whilst the same level of interface pressure is maintained throughout slipping. The research provides a basis for the optimisation of interference-fit design in order that the working lives of expensive shafts, which are prone to damage through ploughing, and brittle hubs, which are prone to sudden fracture, are maximised when experiencing recurrent slipping.*

**Keywords:** *Interference-fit; interface pressure; coefficient of friction; experimental testing; neutron diffraction.*

## 1. INTRODUCTION

Interference-fits are a type of joint consisting of a shaft and a hub. The shaft diameter is manufactured larger than the hub bore diameter creating an overlap or dimensional interference between the two interfacing component surfaces. The joint is then held together by friction and elastic compression. Failure of the joint occurs when it can no longer resist an external load and total slip occurs at the interfaces. The load can be applied via torsion of the shaft within the hub, an axial load, or a combination of the two. A shrink-fit is a special type of heavy interference-fit formed by either heating the outer element, cooling the inner element, or for large interferences, a combination of both. The parts are then returned to ambient temperature to complete the assembly. This avoids surface damage and eliminates the large forces required to assemble other types of interference-fits like press-fits. Interference-fits are commonly used for locating parts (bearings, gears, train wheel tyres), in situations where the compressive stresses are advantageous (gun barrels, pressure vessels), or for transmitting torque (gears, wheels, tool holders). In torque transmission, interference-fits excel over traditional keyways, pins, splines and other assembly methods, as no other components and associated invasive machined features on the parts are required.

In previous work using a statistically large sample size of 27 mild steel interference-fitted shafts (diameter 22 mm) and hubs (diameter 60 mm) (Booker *et al.*, 2004), it was observed experimentally that the failure load to create total slip in torsion, known as the holding torque, increased noticeably when repeatedly loaded (see Figure 1). Using statistical hypothesis tests, the holding torque distribution after just three independent loading cycles to total slip was statistically different, to a high level of significance, from that of the first loading cycle. This phenomenon is an advantage in applications where the main objective is to resist torque – and can be regarded as ‘torque strengthening’. However, repeated slipping can result in wear at the interface of the shaft and hub. In some applications, for example, in large rolls for the hot rolling industry (McMillan *et al.*, 2013) the hub is used like a replaceable tyre possessing different mechanical and thermal properties to the shaft. This is cost effective as the hub can be replaced when worn without having to replace the whole component. Excessive wear of the shaft can be costly though and Figure 2 shows an example of

'ploughing' damage on an alloy steel shaft used in a large work roll assembly. In these situations, shafts can be redressed and reused up to six times during their working life to remove the damage, but when ploughing is severe and deep, the amount of machining required to resurface the roll is impractical and the shaft becomes unusable. As the shaft is the most expensive part of the roll assembly, this type of failure is costly.

The aforementioned failure occurred in a profiled work roll where the hub had been machined down significantly over time and had failed through fracture. At this point in a roll's life, the holding torque will have been reduced significantly due to the reduced interface pressure caused by the removal of hub material, leading to a higher likelihood of slip. As material was removed, the roll became more susceptible to crack propagation initiated through fire-cracking during the intense heating and cooling encountered in the hot-rolling process. The most profound area of ploughing in the case described was found near the boundary of the thick section of the hub. At this point the interface pressure increases due to edge effects caused by the increase in bulk material. This increased interface pressure further increased the effects of wear. The hub, not shown, had fractured in a brittle and sudden manner, exposing the damaged shaft surface. The hub was made from Spheroidal Graphite Acicular Cast Iron (SGACI) which was considerably harder than the alloy steel shaft material.

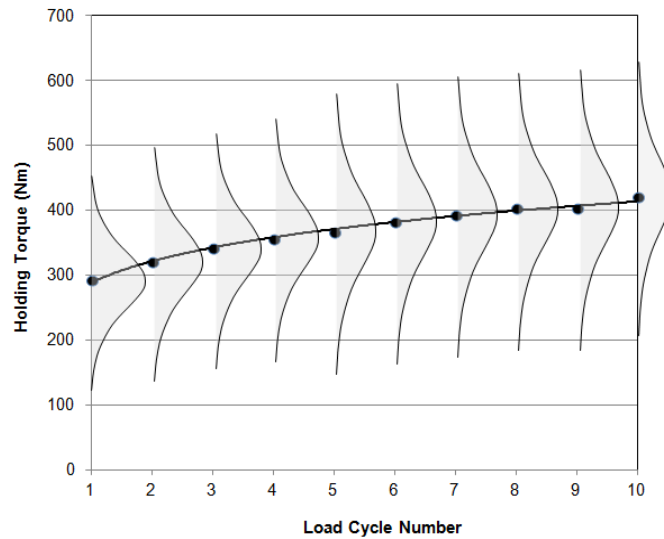


**Figure 1 Distributions of holding torque based on 27 mild steel interference-fitted assemblies (diameter 22mm shaft, diameter 60mm hub) after 10 loading cycles showing increasing mean and similar dispersion**



**Figure 2 Example of severe ploughing damage on an alloy steel shaft taken from a large hot rolling work roll (diameter ~1000mm)**

Ploughing occurs due to the interfacing surfaces sliding against one another while in the presence of a high contact pressure. The peaks of the surface asperities, imparted by machining of the surfaces to create the interference dimensions on the shaft and hub, meet and deform both elastically then plastically to support the typically high contact pressure. The amount of deformation is dependent on the relative hardness of the interfacing materials and the level of interface pressure. As the two surfaces slide against each other the initial contact points begin to separate and large shear forces develop below the contact points. These forces are enough to deform the asperities and even fracture them. When asperities fracture, broken asperities can become trapped in the interface and cause further damage through a prow and wedge type junction (Cocks, 1966; Antler, 1964). This forms the basis for ploughing and has been observed in interference-fits previously (Macdonald, 1971).

The objectives of this paper are to determine the fundamental reasons for an observed increase in holding torque with recurrent slipping in interference-fitted assemblies such as the case of a work roll described above. The paper initially reviews the theory of failure of interference-fits in torsion to understand the dominant parameters in their design and failure. The experimental approaches are then described including a description of the test sizes, materials and rationale for testing. The test results and analysis are presented and discussed before final conclusions from the work are presented together with future research in this area.

## **2. ANALYSIS OF INTERFERENCE-FITS**

### **2.1 Theory and Key Parameters**

The well-established analytical approach used to model the holding torque is based on the thick cylinder theory developed by Gabriel Lamé (Clapeyron & Lamé, 1833). Full derivations can be found in engineering texts (Juvinal, 1967; Timoshenko, 1970). In the case where the shaft and hub materials are dissimilar, omitting stress concentration effects, and with reference to Figure 3, the interface pressure,  $p$ , is given by:

$$p = \frac{\delta}{\frac{R}{E_1} \left[ \left( \frac{R_o^2 + R^2}{R_o^2 - R^2} \right) + \nu_1 \right] + \frac{R}{E_2} (1 - \nu_2)} \quad [1]$$

Where  $\delta$  is the radial interference,  $R$  is the shaft radius,  $R_o$  is the hub outer radius,  $E_1$  is the Young's Modulus of Elasticity for the hub material,  $E_2$  is the Young's Modulus of Elasticity for the shaft material,  $\nu_1$  is the Poisson's ratio for the hub material and  $\nu_2$  is the Poisson's ratio for the shaft material.

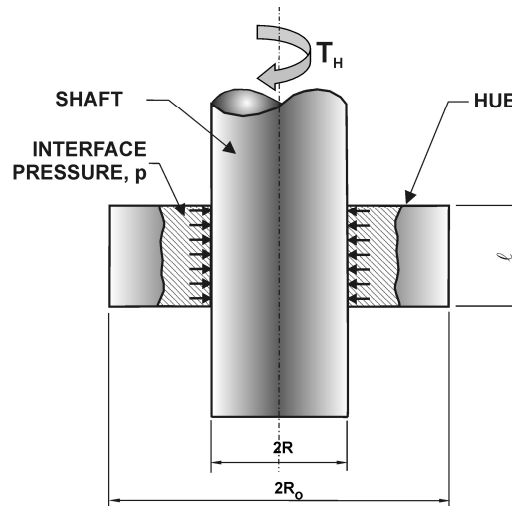


**Figure 3 Schematic of a typical interference-fit under torsional loading (with notation)**

The holding torque,  $T_H$ , is found by using the classic friction formula and adapting it to a cylindrical surface using the radius,  $R$ , as the moment arm (Faupel, 1981).

$$T_H = 2\pi R^2 l p \mu \quad [2]$$

Where  $\mu$  is the static coefficient of friction,  $N$  is the normal force and  $l$  is the length of interfacial contact.

The parameters in the holding torque equation [2] are related to component dimensions, material properties and the coefficient of friction. However, the coefficient of friction, in particular, is a complex parameter: not constant - subject to wide variability, correlated to the interface pressure, and dependent on material hardness/elasticity, surface roughness, surface conditions (dry, lubricated,

oxidised etc), environment (temperature, humidity) and loading rate. These parameters can all affect the measured value (Haehner, 2002; ESDU, 2007). The pressure and contact area may also be affected by geometrical inaccuracies caused by the chosen manufacturing process. Evidence from previous statistical investigations of interference-fitted assembly failures showed that the variation in the coefficient of friction is the most dominant single parameter, contributing up to 50% of the variation in the holding torque observed experimentally (Booker *et al.*, 2004; Booker & Truman, 2008). The coefficient of variation of friction (CoV), being the standard deviation divided by the mean of the measured variate, can be greater than 20% indicating a large dispersion statistically speaking. Compare this to a CoV of 3-5% for a ductile material's tensile properties, for example, its Young's Modulus or yield strength (Haugen, 1980). The remaining contribution to the variation in holding torque is provided by the pressure at the interface through a combination of the chosen dimensional interference and the material's elastic properties as described in equation [1].

## 2.2 Experimental Approaches

Three experiments were conducted to investigate the phenomenon of torque strengthening in interference-fits:

- Experimental testing of small scale interference-fitted assemblies with nominal shaft diameters of 16 mm and 50 mm (63 specimens in total) to measure the holding torque over a range of loading frequencies (total number of slips). All of the specimen shafts were made from alloy steel and the hubs were made from SGACI, emulating the materials used in hot rolling work rolls (see Figure 4). The difference in geometry of the two specimen sizes was mainly due to the different experimental set-ups (drive and constraint fixtures), and torsional test machine capabilities needed for slip testing. The aspect ratios of the most important geometrical features were maintained (shaft outer diameter, hub inner diameter and contact length)
- Neutron diffraction experiments were used to observe the stress state before and after multiple loading frequencies in small scale diameter 16 mm interference-fitted assemblies of an alloy steel shaft with an SGACI hub.



- Novel fracture tests of the 50mm diameter interference-fitted SGACI hubs were conducted to measure the interface pressure following testing. This also provided a secondary verification of the interface pressure using the crack compliance method, which uses the critical crack length at failure to verify calculated values of the internal stress state from analytical equations and finite element models.

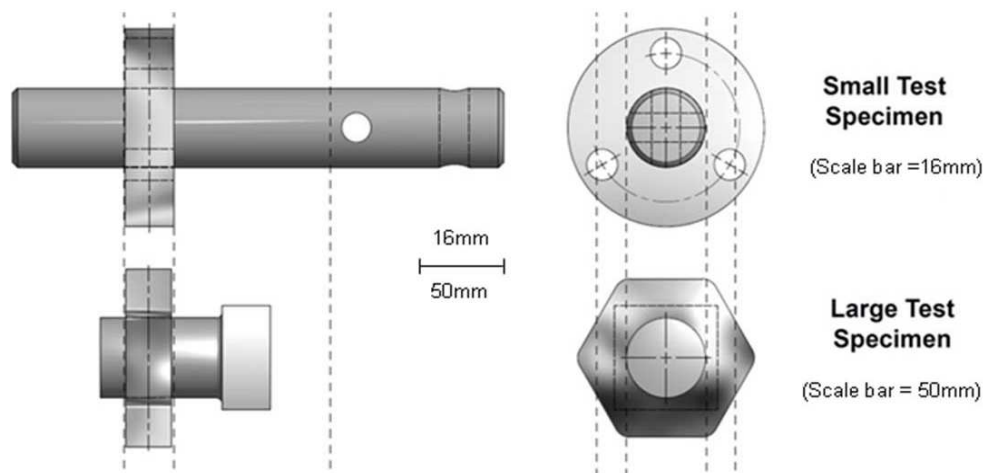


**Figure 4 Experimental interference-fit specimen configurations: diameter 16mm specimen (top) and diameter 50mm specimen (bottom)**

The experiments were designed to test whether increases in the holding torque could be attributed to either interface pressure or friction. Holding torque tests were used to provide a quantifiable observation of the increase in holding torque and provide specimens for further testing using neutron diffraction and fracture tests. The neutron diffraction experiments used two specimens: one which had been tested repeatedly to holding torque failure and a control sample which had not been subjected to torsion. The neutron diffraction method would measure the internal stresses in both samples and show if there was an increase in the radial stress (and therefore, interface pressure) near the interface compared to theoretical and Finite Element Analysis (FEA) predictions. Finally, the 50mm diameter specimens would serve a secondary purpose, using the crack compliance method to verify the internal stress state leading to fracture of a brittle hub.

### 2.2.1 Holding Torque Experiments

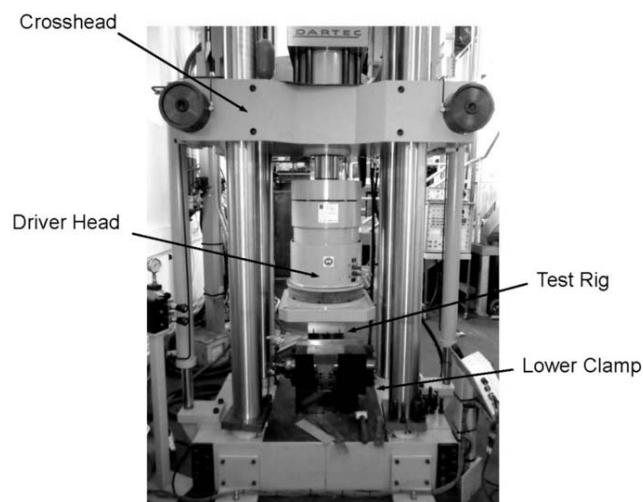
Dissimilar materials were used to replicate a common application of interference-fits where a hard, wear resistant material is used for the hub and a tough, fracture-resistant material is used for the shaft. In this work, SGACI was used for the hub and EN9 (BS 970-1, 1996) steel was used for the shaft. Full material composition and material property tables can be found in (McMillan *et al.*, 2013). Two specimen sizes were used with nominal shaft/hub interface diameters of 16 mm and 50mm. The smaller specimens consisted of a 16mm diameter shaft interference-fitted to a hub with a 40mm outer diameter and a 16mm diameter bore. The contacting surfaces were machine turned to a specified surface roughness of 0.6–1.8  $\mu\text{mRa}$ . A target interference of 0.8-0.9 $\mu\text{m/mm}$  of the shaft diameter was used. However, in practice this was difficult to achieve with the required interferences being between 12.8 $\mu\text{m}$  and 14.4 $\mu\text{m}$ . As a result, there was a larger statistical spread in the interference, and therefore higher than anticipated interface pressures in some of the specimens. The small specimens were tested using a Roell Amsler HCT 25 tension-torsion machine capable of applying a vertical load of  $\pm 25$  kN and a torque of  $\pm 500$  Nm about the vertical axis.

The larger specimens used a hexagonal geometry to secure the specimens in the rig without using bolts or pins, and are large enough not to superimpose a stress field on the interface with the shaft due to the non-uniform shape. The hub outer dimensions were a hexagon of 110mm across face and the hub bore had a diameter of diameter 50 mm with a specified surface roughness of 0.6-1.8  $\mu\text{mRa}$  (measured using a Talysurf). Like the small scale specimens, the interference-fit was defined using a hub basis interference-fit. The hubs were machine turned to roughly 50 mm diameter then a shaft was turned to match the hub. The critical dimensions were measured using micrometers, bore micrometers and an optical comparator. An interference of 0.8-0.9 $\mu\text{m/mm}$  was used and the specimens were tested on a Dartec 500 kN tension-torsion machine capable of applying  $\pm 500$  kN force and  $\pm 20$  kNm torque (see Figure 5).

The testing regime for both specimen sizes was to load the specimen in torsion until the holding torque was exceeded and the shaft slipped within the hub. Once holding torque failure was achieved

the specimen was unloaded and then loaded again until failure. The specimens were loaded to failure a varying number of times, from as little as one holding torque failure to over 100. During testing the hub was fixed to the test rig and the shaft was driven by the testing machine. The free end of the shaft was not constrained as this represented the most likely scenario in real-life applications. An extension arm was attached to the free end of the shaft and was used to load a dial gauge. This provided an instant visual indicator that slip had occurred as the dial gauge jumped when it registered slip in the free end of the shaft. The data logger used by the test machine provided a secondary indicator as well as the experimental measurements used in the analyses.

a)



b)

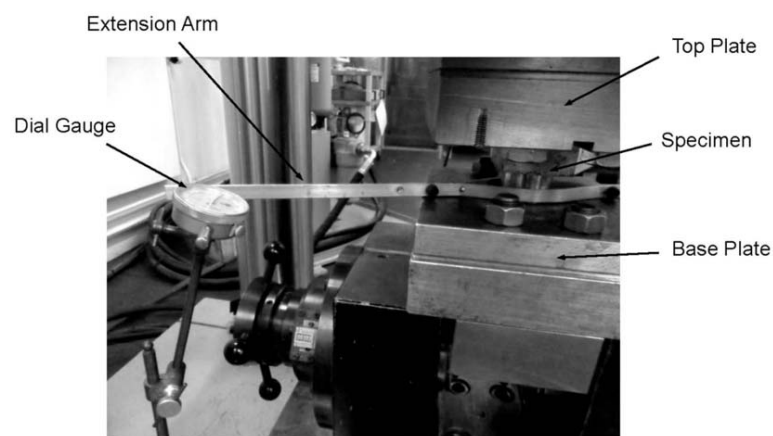


**Figure 5 Experimental test set-up for large interference-fit specimens (50mm) using Dartec torsional loading platform**

### 2.2.2 Neutron Diffraction Experiments

Neutron diffraction is a technique for studying the structure of materials through elastic scattering. In the engineering sector, it is used to define the elastic stress state in a component by measuring the lattice strains. In effect, the crystal lattice can be used as a strain gauge by comparing the lattice spacing in a stressed sample to the lattice spacing in an unstressed reference sample. Bragg's law of diffraction states that when an incoming wave or particle has a wavelength of comparable size to the inter-atomic spacing, constructive interference of the scattered wave or particle will occur when the following conditions are met (Tipler & Mosca, 2004):

$$2d\sin\theta = n\lambda \quad [2]$$

Where  $d$  is the lattice spacing between crystal planes,  $\theta$  is the scattering angle,  $n$  is an integer value denoting the order of reflection and  $\lambda$  is the wavelength of the incoming wave/particle. The only unknown variables are  $d$  and  $\theta$ , so by examining the scattering angle required to satisfy Eq. [3], the lattice spacing can be calculated.

In order to find the strain in a component, reference measurements need to be taken in stress free samples so the strain in the stressed component's crystal lattice can be compared to the strain in a stress-free reference sample. This is found from [4]:

$$\varepsilon = \frac{d - d_0}{d_0} \quad [3]$$

Where  $\varepsilon$  is the strain and  $d_0$  is the lattice spacing in the unstressed reference sample. Once the strain is known, the stresses can be calculated using generalised Hooke's law. To complete the terms of the

stress tensor, six strain measurements are required. However, if the principal directions are known, the stresses can be calculated with only three strain measurements (Fitzpatrick, 2003):

$$\sigma_{RR} = \frac{E}{(1 + \nu)(1 - 2\nu)} [(1 - \nu)\varepsilon_{RR} + \nu(\varepsilon_{\theta\theta} + \varepsilon_{zz})] \quad [4]$$

$$\sigma_{\theta\theta} = \frac{E}{(1 + \nu)(1 - 2\nu)} [(1 - \nu)\varepsilon_{\theta\theta} + \nu(\varepsilon_{RR} + \varepsilon_{zz})] \quad [5]$$

$$\sigma_{zz} = \frac{E}{(1 + \nu)(1 - 2\nu)} [(1 - \nu)\varepsilon_{zz} + \nu(\varepsilon_{RR} + \varepsilon_{\theta\theta})] \quad [6]$$

Where E is the Young's modulus,  $\nu$  is Poisson's ratio and  $\varepsilon_{rr}$ ,  $\varepsilon_{zz}$  and  $\varepsilon_{\theta\theta}$ , are the strains in the principal directions. Using a cylindrical coordinate system the principal strains are R,  $\theta$  and Z for the interference-fit assemblies. The measurement paths used to access the principal strain directions are shown in Figure 6.

The neutron measurements were taken using the Strain Analyser for Large and Small scale engineering Applications (SALSA) at the Institute Laue-Langevin, Grenoble, France. SALSA is a monochromatic strain diffractometer situated on a reactor-based neutron beam line (Pirling, Bruno, & Withers, 2006). The high neutron flux of reactor-based sources allows measurements to be taken deeper within the material and still provide good results.

Two diameter 16mm SGACI/EN9 specimens were chosen for the tests as described in the previous section due to their smaller size being easily accommodated in the SALSA equipment. One specimen had been slipped 20 times and had an interference-fit of 17.4  $\mu\text{m}$  (averaged measurement around the circumference, giving around 80MPa interface pressure); the other specimen was untested, as-assembled and had an interference-fit of 16.6 $\mu\text{m}$  (averaged measurement around the circumference, giving around 76 MPa interface pressure). The initial holding torque of the slipped specimen was found to be 10.92 Nm increasing to 19.43 Nm after 20 slips. The two specimens were examined using neutron diffraction to determine whether or not the stress state changed following repeated failures. An observed change in stress state would indicate a change in interface pressure, suggesting that the interface pressure was dominating the increase in holding torque.

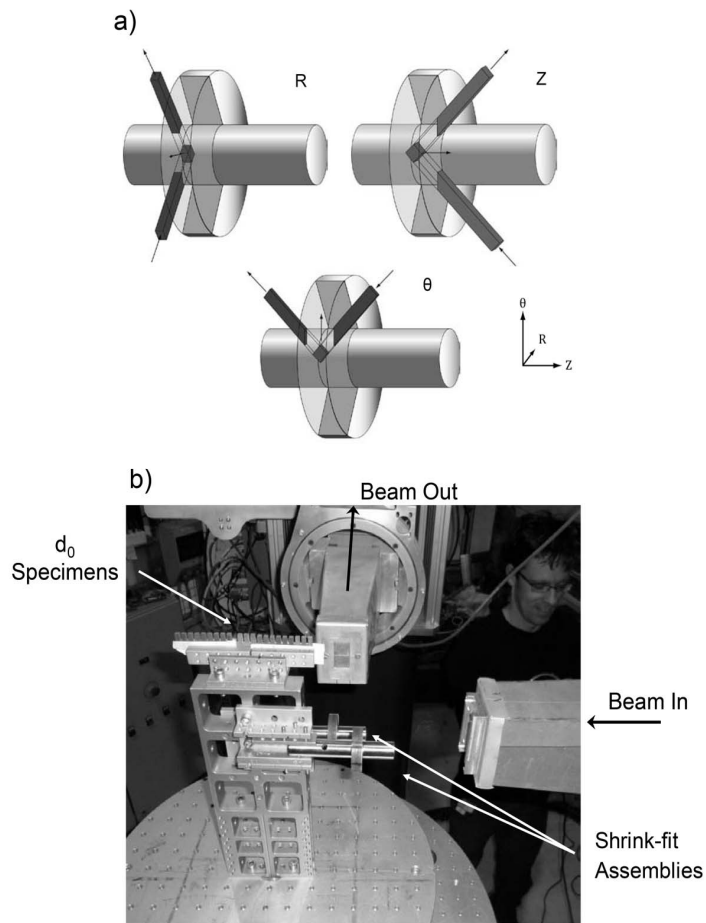


**Figure 6 Neutron diffraction measurements of residual stress in diameter 16mm SGACI hub/alloy steel shaft specimen, a) measurement paths, b) experimental set-up for interference-fit assemblies**

In total, 16 measurement sites were used through the radius of the interference-fits: 5 positions in the shaft and 11 positions in the hub. A gauge volume of 0.6mm x 0.6mm x 2mm was chosen. In order to keep the gauge volume away from the interface, measurements were not taken within 1mm of the interface or outside edge of the specimen to avoid erroneous results caused by the gauge volume

overlapping the interface. Reflections were measured from the [2, 1, 1] crystal plane for  $\alpha$ -ferrite. The [2,1,1] plane is the most isotropic plane for body-centred cubic crystal structures like  $\alpha$ -ferrite (Fitzpatrick, 2003) which means the diffraction elastic constants are close to the bulk elastic constants of ferritic steels.

To create a stress free sample from which to take  $d_0$  measurements, a set of reference combs were cut by a wire electric discharge machine (EDM) from the materials used to make the samples. By cutting small combs into the material it is intended that the elastic strain will be released due to lack of constraint from the bulk material. However, the lattice spacing can be affected by events in the material's usage history such as any plasticity or heat treatment, so it is important to cut the reference samples from the same material, preferably with the same orientation of the measured sample. In the EN9 shafts, one reference comb was cut from a shaft from the same batch as the specimens used. As the material used was provided as a hot rolled bar which was machined to size, there should be very little residual stress within the material. The comb was cut from the centre of the shaft in the axial direction. The SGACI reference combs were cut from the material blanks used to create the hubs. A reference comb was cut from each blank so that the  $d_0$  values could be compared.

### 2.2.3 Fracture Toughness Tests

Fracture toughness is a material property which describes the ability of a material to resist brittle fracture when a crack is already present. The fracture toughness is derived from the stress intensity factor approach to fracture mechanics (Anderson, 2005). The stress intensity factor,  $K$ , is given by:

$$K = f\sigma\sqrt{\pi a} \quad [7]$$

Where  $f$  is the non-dimensional stress intensity factor,  $\sigma$  is the remote applied stress and  $a$  is the crack length.

If the fracture toughness is known accurately then the failure loads and initial stresses can be calculated based on the crack length at failure. In this work, the fracture toughness of the SGACI material was measured using compact tension (C(T)) specimens. C(T) specimens were designed following the ASTM E1820 standard (ASTM, 2011) for fracture toughness testing. The C(T) specimens were tested using an Instron 1342 hydraulic test machine with a load capacity of 250 kN. Instron Wavemaker and Waverunner software were used to control the test machine and capture data from both the test machine and the clip gauge, which was used to measure the crack tip opening displacement (CTOD). A calibrated Instron 2670-116 COD clip gauge was used to measure the CTOD. The gauge was zeroed before the tests using a barrel micrometer in conjunction with the Instron software.

The fracture toughness was calculated using:

$$K_{IC} = \frac{F_Q}{B\sqrt{W}} f(a/W) \quad [8]$$

Where  $f(a/W)$  is a shape factor function with a polynomial term. The shape factor is provided by (Anderson, 2005):

$$f(a/W) = \frac{\left(2 + \frac{a}{W}\right)}{\left(1 - \frac{a}{W}\right)^{\frac{3}{2}}} \left[ 0.866 + 4.64 \frac{a}{W} - 13.32 \left(\frac{a}{W}\right)^2 + 14.72 \left(\frac{a}{W}\right)^3 - 5.60 \left(\frac{a}{W}\right)^4 \right] \quad [9]$$

For the SGACI material, the average fracture toughness value was found to be 43.4 MPa.m<sup>1/2</sup>. Using the results of the fracture toughness tests, the diameter 50mm specimens described previously, which had undergone repeated slip, were fractured so that the interface pressure could be calculated based on the crack length at failure. This provided a second method for validating whether or not the interface pressure had changed following repeated slips.



To create the cracks the specimens were placed in the EDM machine which created a cut using a diameter 0.25mm wire beginning at the mid-plane of the flat edge of the hexagonal interference-fit specimen. This gave a specimen thickness,  $W$  of 24.5mm. The wire was fed into the specimen until the stress intensity factor caused by the crack tip was high enough ( $K \geq K_{IC}$ ) to cause brittle failure of the specimen. At this point the specimens were removed and doused in acetone to preserve the surfaces. The crack length was measured using an optical comparator at 3 points along the fracture surface and the results averaged then subtracted from the specimen thickness,  $W$ , to give the crack length,  $a$ . Finally, the crack length ratio,  $a/W$ , was calculated to compare the experimental results to the analytical and finite element model results.

#### 2.2.4 Finite Element Models

Four models were created using the SGACI, EN3B and EN9 material properties. The models were created in ABAQUS/CAE from the CAD drawings presented in Figure 4 as full, 3D models in a cylindrical co-ordinate system. Two reference points were created at the origin. One reference point was constrained to the hub bore surface in the  $\theta$  and  $z$  linear directions and the  $r$ ,  $\theta$  and  $z$  rotational directions. The reference point was then held by a displacement boundary condition in the Cartesian  $x$ ,  $y$  and  $z$  directions to hold it in place. This allowed the hub to expand and contract during interference-fitting, but constrained movement in the axial direction relative to the shaft. The second reference point was constrained to the end of the shaft at which loading was applied. All degrees of freedom were constrained so that the reference point could fully control the surface. The reference point was then held by a displacement boundary condition in the  $x$ ,  $y$  and  $z$ -rotational directions. To create displacement controlled loading, the reference point had a displacement applied in the  $z$ -rotational direction to apply a torque. The final boundary condition was applied at the hub outer surface to provide resistance to the applied loading.

A surface to surface contact was defined between the hub and shaft surfaces. Geometrical smoothing was used to provide less noisy contact pressure results with curved surfaces. The friction coefficient was defined on a model-by-model basis as determined by the surface preparation of the experimental

tests. Friction was defined using the penalty method and hard contact options in ABAQUS. A mesh convergence study was carried out for both specimen sizes and found that an element size of less than 0.1mm was optimum for the diameter 16mm model and less than 0.5mm for the diameter 50mm model. Linear C3D8 elements were used for the analyses.

Only the 50mm specimens were used in the fracture tests, and so a 3D finite element model was created by importing the hexagonal hub design into ABAQUS/CAE. Nine models were created with crack length ratios between 0.725 and 0.925, increasing in 0.025 intervals. Twenty load increments were imposed to gradually ramp the interface pressure up to 75 MPa with the pressure applied as a uniform pressure distributed over the bore surface. A mesh convergence study found that the optimum element size was between 25  $\mu\text{m}$ .

The global mesh and refined mesh around the crack tip are shown in Figure 7. Each model contained between 18,000 and 20,000 elements, depending on the crack length and partitioning of the mesh. Type C3D20R hexagonal 3D 20-node elements with 8 reduced integration points were used to mesh the model. The contour integral method was used to simulate the crack tip and linear-elastic fracture properties were defined by setting the second order mesh options to collapse the nodes nearest to the crack tip to a single point and move the mid-side nodes to the quarter point of the element. This creates a strain singularity proportional to  $1/\sqrt{r}$ , required for a cracked linear-elastic body.

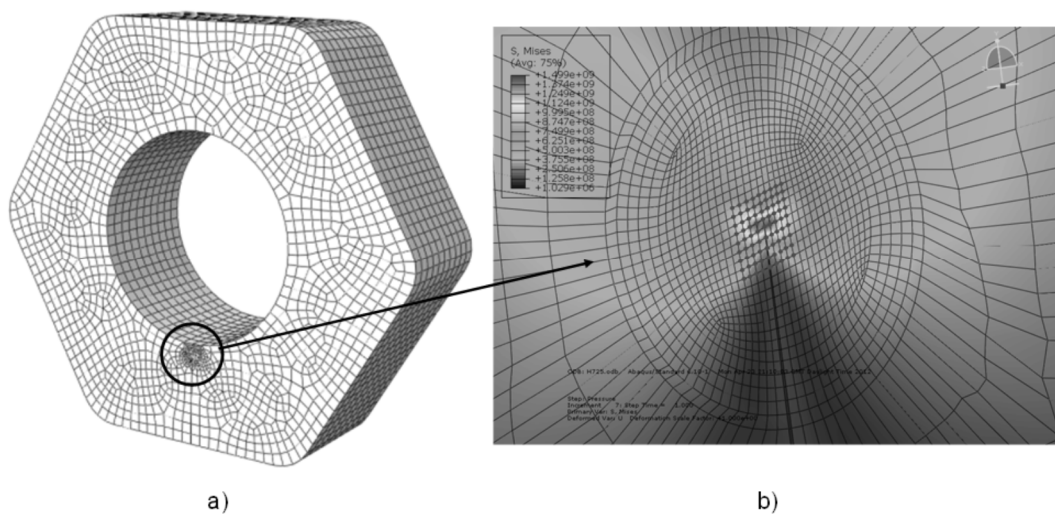


Figure 7 a) FE mesh for critical crack study in hub, b) refined mesh around crack showing contour

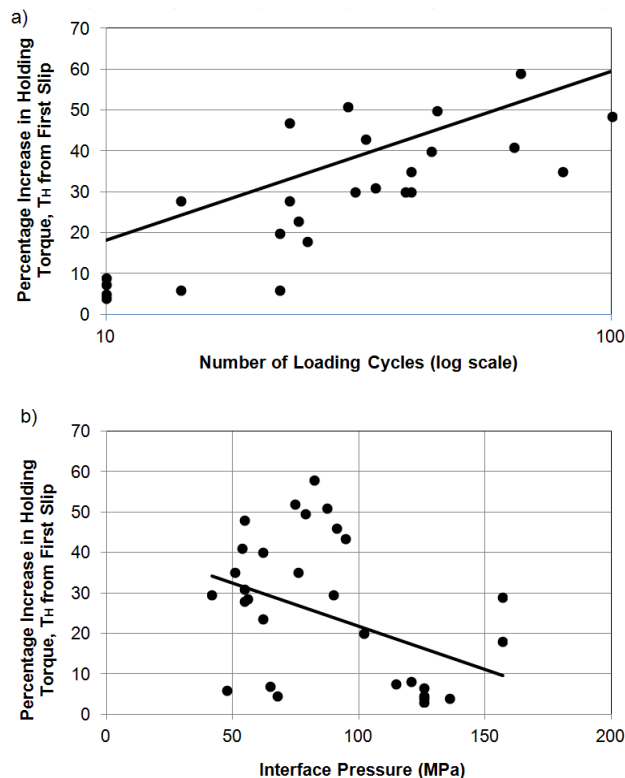
integral region (units: Pa)

A reference point was defined in the centre of the model to which the hub bore was constrained in all directions. This reference point was used to create the boundary conditions through a pin constraint. This allowed the model to expand in the hoop and radial direction, but did not allow it to rotate or translate in the z direction. Stress intensity factor,  $K_I$ , and pressure values were outputted from the model for comparison with the experimental crack tests.

### 3. EXPERIMENTAL RESULTS AND DISCUSSION

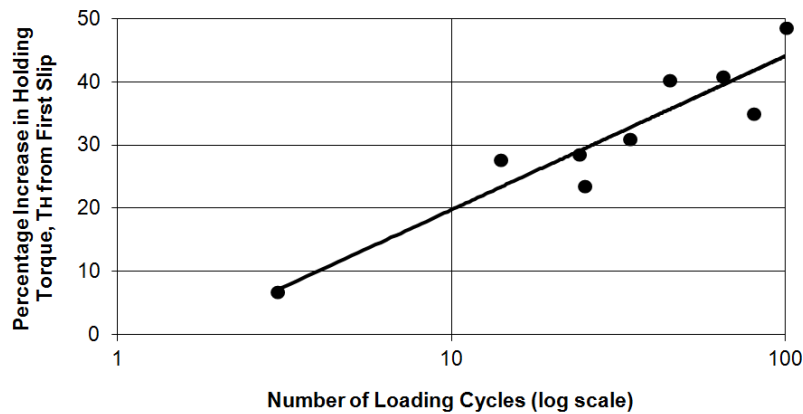
#### 3.1 Holding Torque Experiments

Figure 8a) shows the total increase in holding torque between first and final slips as a percentage value relative to the number of slips (loading cycle) and b) relative to the interface pressure for the diameter 16mm SGACI hub/EN9 alloy steel shafts specimens. It can be seen that there is a strong positive correlation (correlation coefficient,  $r = 0.81$ ) between final holding torque and number of slips. Total torque increase against interface pressure shows a very weak correlation (correlation coefficient,  $r = 0.37$ ).



**Figure 8 Percentage holding torque increase for diameter 16 mm SGACI/EN9 specimens a) as a function of loading cycle number, b) as a function of interface pressure**

The results for the diameter 50mm specimens are shown in Figure 9. The diameter 50mm specimens presented the largest increases in holding torque and most consistent data, although with fewer samples. These specimens were used for further verification of the cause of increase using the crack compliance method (discussed later). Figure 9 shows a strong correlation of the final holding torque value increasing with number of slips for the diameter 50mm specimens (correlation coefficient,  $r = 0.94$ ).



**Figure 9 Percentage holding torque increase for diameter 50mm SGACI/EN9 specimens as a function of loading cycle number**

The coefficient of friction was calculated from the recorded experimental holding torque values on first and last slips for the diameter 50mm specimens. The coefficient of friction can be derived from Eq.[2] as:

$$\mu = \frac{T_H}{2\pi R^2 lp} \quad [10]$$

Figure 10 shows that the coefficient of friction increased from the initial slip to the final slip for the same diameter 50mm specimens. Note that as the interface pressure on first assembly is not constant across all specimens manufactured. However, over the small range of interface pressure created in all specimens, approximately 10MPa, there is direct evidence to suggest that the coefficient of friction

effectively increases with number of slips accordingly. Static coefficient of friction measurements between SGACI and EN9 alloy steel were also determined using a testing method discussed in Booker & Truman (2012). These tests, conducted on statistically relevant sample sizes and under similar pressures and surface conditions, yielded an average coefficient of friction,  $\mu_{av} = 0.433$ , with a standard deviation,  $SD = 0.071$ . Figure 10 also shows the expected value for the coefficient of friction superimposed as a band of width  $\pm 1SD$ , within which sit most of the initial coefficient of friction values back-calculated from the torque measured on first slip.

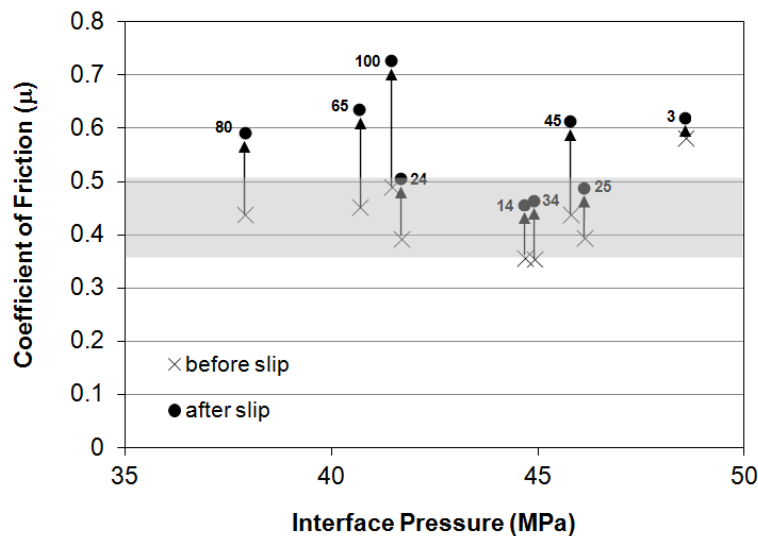


**Figure 10** Coefficient of friction calculated from holding torque for a range of loading cycles to slip (number next to markers) for diameter 50 SGACI hub/EN9 alloy steel shaft specimens (grey band represents measured coefficient of friction  $\pm 1SD$  as a reference)

### 3.2 Neutron Diffraction Experiments

Diffraction peak data were analysed using SALSA's in-house software LAMP (Large Array Manipulation Program). From this, the diffraction angle was obtained and used to calculate the strains and stresses as outlined earlier. The results for the radial scans of both the slipped and un-slipped specimens are plotted and compared to the FE predictions in Figure 11. For reference, the EN9 shaft was located between 0 and 8mm and the SGACI hub was located between 8 and 20mm. In the SGACI material (position  $> 8mm$ ) it can be seen that some measurements deviate dramatically from the predicted values. There were also large errors associated with some of the measurements. In the EN9

material (position < 8mm) the measurements are closer to the predicted values, with smaller error bars.

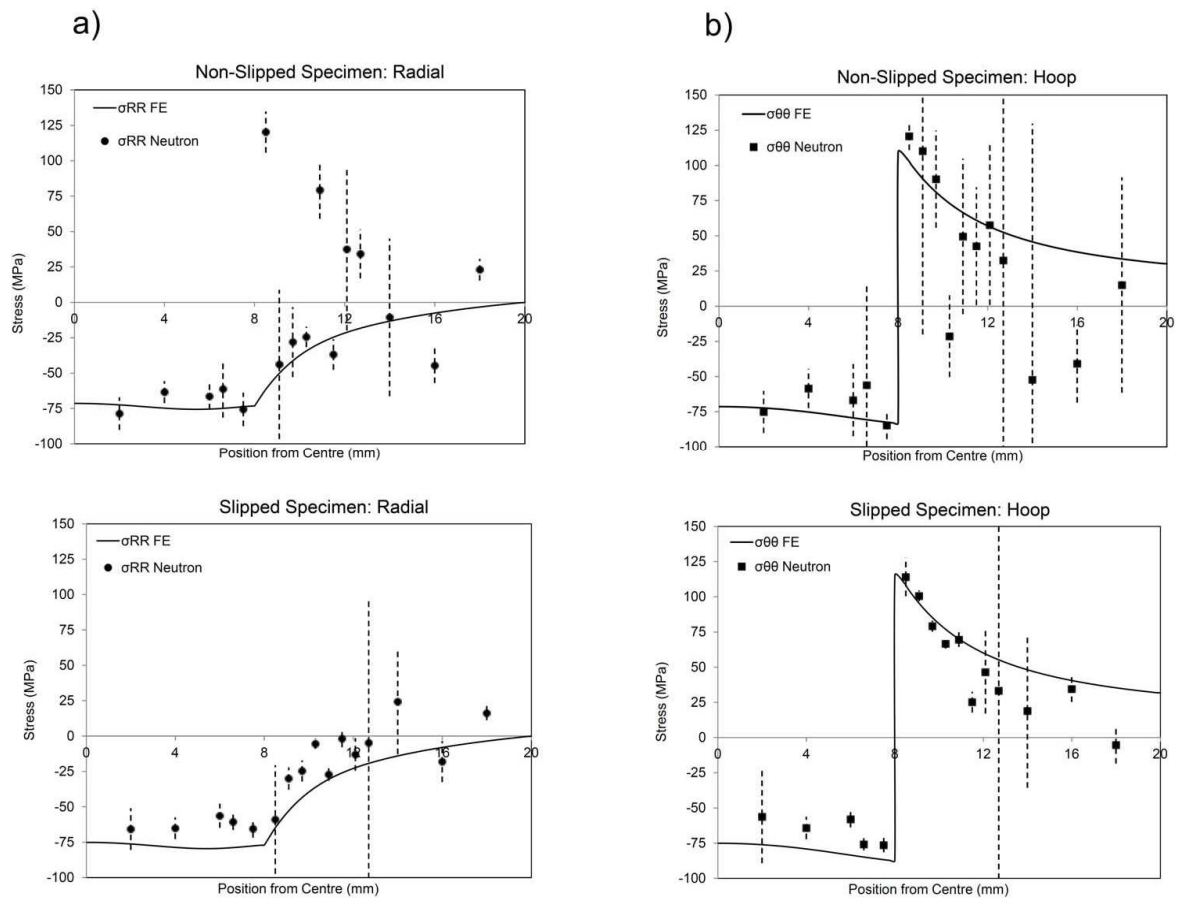


**Figure 11 Hoop (a) and radial (b) stress comparisons for a non-slipped (as assembled) interference-fit and an interference-fit with 20 independent loading cycles to slip applied**

On initial analysis of the data, the EN9 peaks were sharp with good intensity. The data for SGACI material, however, had a large variability in the peak quality and intensity and it was decided to examine the material microstructure for anomalies. Examination of the SGACI material micrographs (Figure 12a) show a bainitic matrix with large carbide content (white in the image) and large, unevenly distributed spheroids of graphite (black). Image analysis showed that the graphitic spheroids ranged from around 40 $\mu\text{m}$  up to 300 $\mu\text{m}$  in diameter with the average size being around 100 $\mu\text{m}$ . The gauge volume used at SALSA was 600 $\mu\text{m}$  x 600 $\mu\text{m}$ , so a large spheroid of graphite or multiple spheroids of graphite within the gauge volume would be problematic for measuring the diffraction angle using a monochromatic beam, as used at SALSA. This is because the hexagonal crystal

structure of the graphite does not have a strong reflection in the (2,1,1) plane chosen for observation (Li & et.al, 2007). As the monochromatic beam was only reflecting from the (2,1,1) plane of the  $\alpha$ -ferrite and carbide, materials that do not reflect from the objective plane will not give a strong reading at the detector. This gave rise to the low intensity of the measured peaks and the data had a large variability. For some points, there were insufficient data for a reliable strain measurement and all points suffered from some interference in the measurement caused by the graphite. This accounts for the poor agreement between the FE prediction and the measurements in the hub material, particularly Figure 11 b): non-slipped specimen hoop stresses.

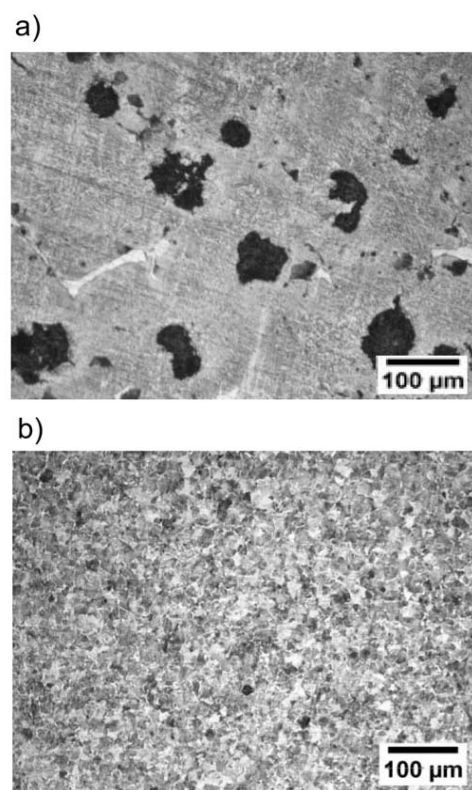


**Figure 12 Microstructure of a) SGACI do specimen material for hub showing large spheroid carbon nodules, compared to b) alloy steel do specimen material for shaft (200x magnification)**

The EN9 microstructure (Figure 12b) was much finer and more evenly dispersed than the SGACI microstructure with grains generally around 10 to 20μm, with a maximum of about 50μm. As the grains were much smaller, the gauge volume contained more grains from which the neutrons were

diffracted, giving a larger sample size for the measurements and providing results which were more representative of the average.

The requirement of the neutron diffraction measurements was to test the hypothesis that the interface pressure was the dominating factor governing the observed increase in holding torque following repeated slipping. The results showed that there was no apparent change in the interface pressure relative to the change in holding torque from the as-assembled interference-fit to one which had slipped 20 times, leading to the conclusion that surface effects and friction must be responsible for the increase in holding torque as suggested by Figure 10. This is because the interface pressure is equal to the compressive stresses in the shaft, and if these stresses had changed following slipping, then the interface pressure could have increased. This effect was not observed in the experiments. The unslipped specimen had a calculated interface pressure of 80MPa. The corresponding average hoop and radial stresses measured by neutron diffraction were 68MPa and 69MPa respectively. The slipped specimen had a calculated interface pressure of 76MPa. The corresponding average hoop and radial stresses measured by neutron diffraction were 66MPa and 63MPa respectively. As the increase in pressure required to create an increase in holding torque proportionate to the experimental holding torque test was around 60MPa, taking the expected interface pressure to 136MPa, it is reasonable to say that the interface pressure, based on neutron experiments, was not the dominating factor in increasing the holding torque.

### **3.3 Fracture Tests**

Following the experimental holding torque testing of the 50mm specimens, the hubs were artificially fractured using the wire EDM process to understand the stress state in the specimens. Figure 13 shows an example fracture surface of a SGACI hub. Two distinct surfaces can be seen: the wire EDM cut is prevalent throughout most of the surface with the final point of the EDM cut visible as a sharp line followed by the fresh, bright fracture surface. The wire EDM process was stopped immediately following fracture of the hub and the crack length was measured. The finite element modelling discussed in Section 2.2.4 was used to predict the critical crack lengths over a range of interface



pressures for each specimen. Figure 14 shows the FE model plots and Figure 15 provides the summary chart used in Table 1 comparing all the experimental, analytical and finite element results. It can be seen that there is a good correlation between the interface pressure and critical crack length and this is independent of the number of the slips the specimen had seen. The critical crack length predicted by the finite element models show good agreement with the experimental studies with an average error of 1.1%. From the results of these experiments, it is reasonable to say that the interface pressure was not the dominating factor in increasing the holding torque.

**Table 1 Critical crack study results**

<b>Specimen No.</b>	<b>Calculated Interface Pressure On Assembly (MPa)</b>	<b>No. Slips Assembly Subjected to</b>	<b>Crack Ratio from Experiment (a/W)</b>	<b>Crack Ratio from FEA (a/W)</b>	<b>Back-Calculated Interface Pressure (MPa)</b>	<b>Interface Pressure Error (%)</b>
1	65	3	0.83	0.82	63.9	1.6
2	62	25	0.84	0.84	62.1	-0.2
3	62	45	0.86	0.84	60.6	2.2
4	55	65	0.87	0.87	54.9	0.3
5	51	80	0.92	0.89	49.7	2.5
6	56	100	0.87	0.87	56.0	0.0

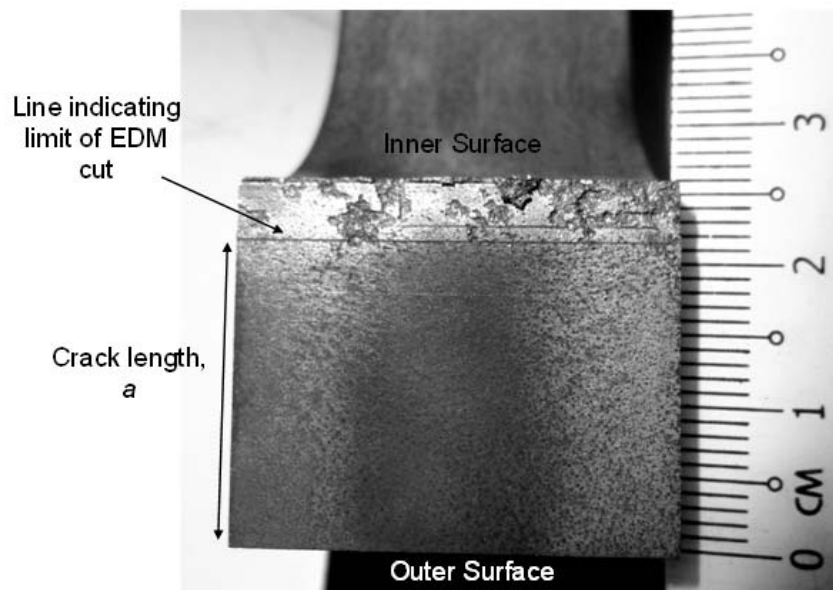


**Figure 13 Cross section of a SGACI hub showing limit of wire EDM cut (crack length) before fracture**

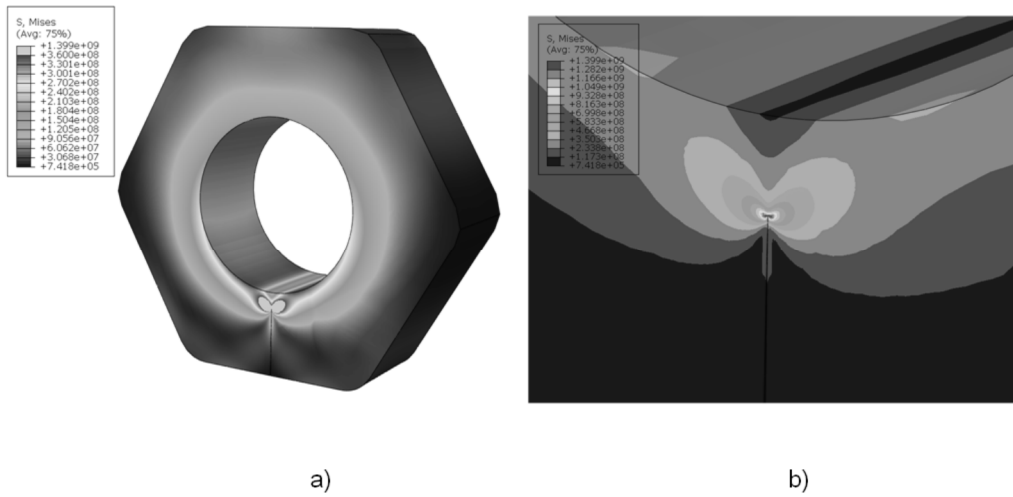


Figure 14 FE model for diameter 50mm hub with crack emulating wire EDM process, a) contour plot with false maximum stress, b) detailed contour plot of the crack tip (units: Pa)

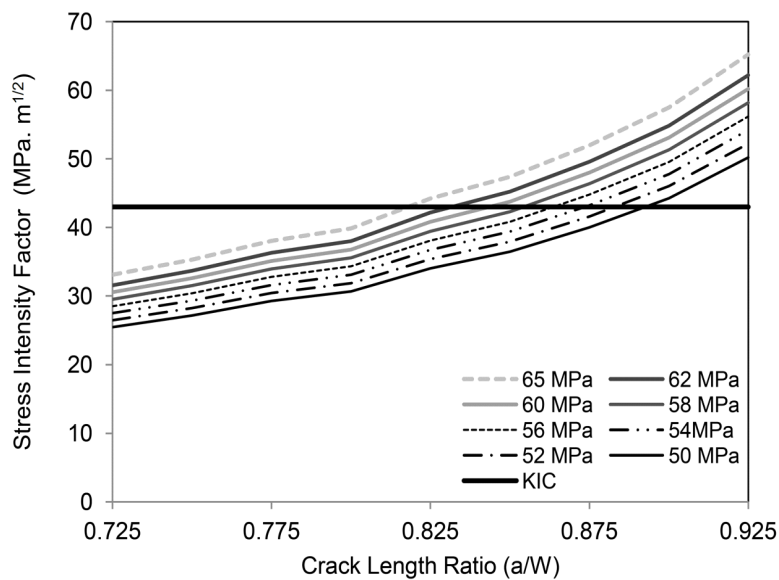
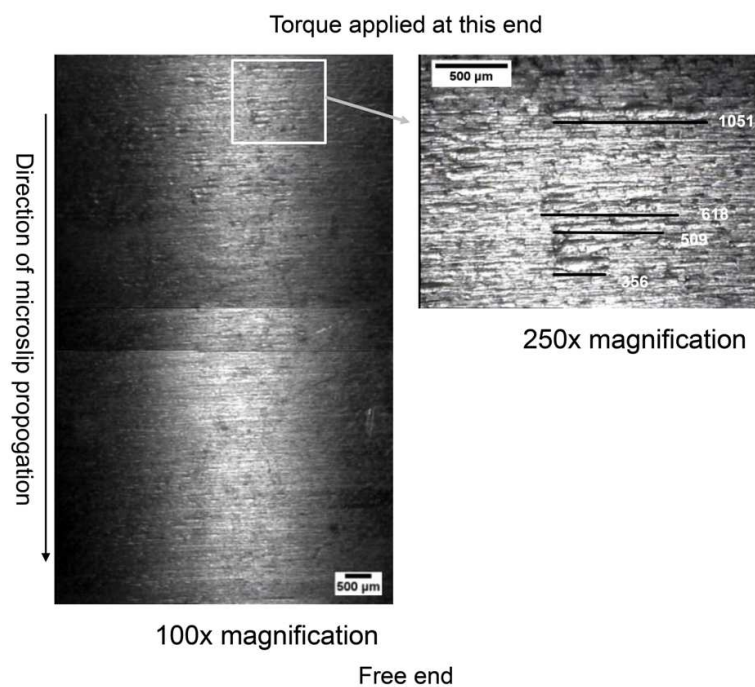


Figure 15 FEA predictions of critical crack length ration in relation to pressure (bold black horizontal line represents the average fracture toughness,  $K_{IC}$  for SGACI hub material)

### 3.4 Examination of Shaft Surfaces

In addition to the experiments, analyses and FEA studies described above, and considering that ploughing had been observed on shaft surfaces in previous studies and failed work rolls, wear

examinations were conducted to find evidence of ploughing on the shaft surfaces of the test samples. Figure 16 shows this evidence in a high magnification photograph of one of the specimen shafts (diameter 50mm). In fact all shafts had undergone a significant amount of ploughing following repeated slipping. The ploughing is the only change in surface condition which could have increased the coefficient of friction to account for the increasing holding torque observed in the specimens. In some instances, large scale ploughing had occurred and destroyed the hub surfaces too and this was much more prominent in specimens that had undergone 45 repeated failures, with plough features in some cases being recorded over 1mm in length as shown in the higher magnification image at the right hand side of Figure 16. An interesting observation is that the length of ploughing is at a maximum at the end of the shaft where the torque is applied. This may be due to microslip damage. Microslip will begin at the end where torque is applied and advance along the contact interface until full holding torque failure is reached.



**Figure 16 Ploughing wear on an alloy steel shaft surface from a diameter 50mm specimen**

To determine the degree of ploughing on multiple slips, a Talysurf surface roughness measuring device was used to measure the surface roughness of several specimen component surfaces (shafts and hubs) over the interface lengths. Figure 17 shows the results, where the figures on the left relate to the change in shaft roughness from that before assembly to first slip, and the figures on the right hand

side, before assembly to 109 slips. It is clear that the surface roughness has changed markedly on the shaft from that measured on the shaft before assembly to even just a single slip. Asperities and machine marks disappear and are replaced by large peaks and troughs on the surfaces (plough features) towards the driven end of the shaft, this being more pronounced on the specimen which has been slipped 109 times.

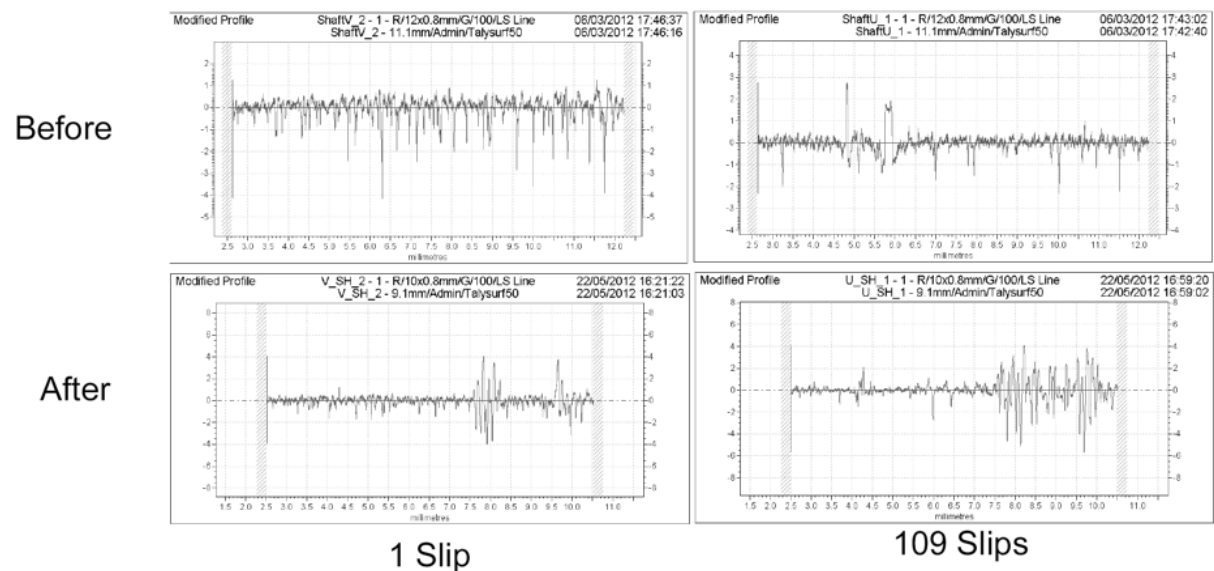


**Figure 17 Comparison of the alloy steel shaft surface roughness along the length of the interface with SGACI hub, before and after first slip (left) and before and after 109 slips (right) (torque applied to shaft on right hand side relative to charts)**

#### 4. CONCLUSIONS

The aim of this research was to identify the reason for an observed increase in holding torque in interference-fitted assemblies when subjected to a multiple, independent loadings to failure. Previously, studies have shown that the interface pressure and coefficient of friction are the major contributors to the holding torque, so these parameters were the focus for a range of experimental tests, analyses and finite element models.

Neutron diffraction experiments on a virgin (as assembled) test specimen and a specimen that had been repeatedly slipped 20 times showed no discernible change in the stress state of the samples

suggesting that there was no change in the interface pressure when the specimen had repeatedly failed. Novel crack compliance tests yielded similar results when testing the hypothesis that an increase in interface pressure occurred with repeated slips. No correlation was evident, and even when specimens reached 100 slips, the interface pressure remained essentially the same, within reasonable error, from that determined on initial assembly of the shaft and hub.

Experimentally, it was found that when 100 slips had taken place, the holding torque to fail the assembly in total slip had increased from that observed on first slip by approximately 50%, for specimen sizes of 16mm and 50mm nominal shaft diameter. Calculations comparing the coefficient of friction from first to multiple slip conditions indicated that large increases occurred in order to account for the observed large increase in holding torque given that no other ‘strengthening’ mechanism took place during slipping. Ploughing was observed on all specimen shafts at the interface with the hub, and in some cases, ploughing on the hub was observed too. Surface roughness measurements on the shafts confirmed the change of surface state before assembly and after slip. Ploughing as a wear mechanism provides no additional pressure to the interface, but effectively increases the coefficient of friction on multiple slips, accounting for the increase in the measured holding torque.

This ongoing research provides new quantifiable knowledge in the area and presents an opportunity to optimise interference-fitted assemblies, particularly in applications where the shaft is to be reused and it is advisable to limit the number of repeated holding torque failures to limit the amount of damage to the shaft. In the context of hot-rolling work rolls, the working life of the more expensive shaft component is to be maximised so ploughing damage must be kept to a minimum. It is hoped this work will give a better understanding of the contributing factors and methods with which to limit destruction of the shaft surface from ploughing damage. Future work will explore optimisation approaches for hot working rolls and other applications where interference-fits are the preferred solution for transmitting torque and sustaining axial forces in machines and production equipment.

## Acknowledgements

This work was supported by the Engineering and Physical Sciences Research Council (EPSRC) and TATA Steel under iCASE grant no. 08000726, *Optimising the Performance of Interference-fitted Sleeves for Rolls in Hot Long-product Rolling*. Thanks are extended to Steve Moir of TATA Steel for his help with the failure case.

In memoriam of David Smith who sadly passed away during the writing of this paper.

## References

- Anderson, T. L. (2005) *Fracture Mechanics: Fundamentals and Application*. CRC Press, Boca Raton, FL.
- Antler, M. (1964) Processes of Metal Transfer and Wear. *Wear*, **7**, 181–203.
- ASTM. (2011). ASTM E1820 - Standard Test Method for Measurement of Fracture Toughness, ASTM International, West Conshohocken, PA.
- Booker, J. D., Raines, M. & Swift, K. G. (2001) *Designing Capable and Reliable Products*. Butterworth-Heinemann, Oxford.
- Booker, J. D., Truman, C. E., Wittig, S. & Mohammed, Z. (2004) A Comparison of Shrink-fit Holding Torque using Probabilistic, Micro-mechanical and Experimental Approaches. *Proc. Instn. Mech. Engrs., Part B*, **218**, 175-187.
- Booker, J. D. & Truman, C. E. (2008) A Statistical Study of the Coefficient of Friction under Different Loading Regimes. *Journal of Physics D: Applied Physics*, **41**(17), 174003.
- Booker, J. D. & Truman, C. E. (2011) Measuring the Coefficient of Friction for Use in Shrink-fit Calculations. *Experimental Techniques*, **35**(2), 7-13.
- BS 970-1 1996 (1996) British Standard for Carbon Steel Specifications.
- Cocks, M. (1966) Shearing of Junctions between Metal Surfaces. *Wear*, **9**, 320–328.
- ESDU (2007) ESDU Guide 68002 Shafts with Interference-fit Collars, Part 1: some factors affecting the design of an assembly. Engineering Sciences Data Unit (ESDU) International plc, London.

- Faupel, J. H. (1981) Engineering Design. Wiley, New York.
- Fitzpatrick, M. E. (2003) Analysis of Residual Stress by Diffraction using Neutron and Synchrotron Radiation. CRC Press, Boca Raton, FL.
- Haehner, C. L. (2002) Coefficient of Friction Measurements, NASA Materials Engineering Branch Document No. 069.  
([https://code541.gsfc.nasa.gov/Uploads\\_materials\\_tips\\_PDFs/TIP%20069R.pdf](https://code541.gsfc.nasa.gov/Uploads_materials_tips_PDFs/TIP%20069R.pdf)) Viewed 27/08/2015.
- Haugen, E. B. (1980) Probabilistic Mechanical Design, Wiley Interscience, New York.
- ISO/IEC (1998) Guide to the Expression of Uncertainty in Measurement (GUM) – Guide 98. ISO, Switzerland.
- Juvinall, R. C. (1967) Stress, Strain and Strength. McGraw Hill, New York.
- Clapeyron, B. P. E. & Lamé, G. (1833) Mémoire Sur L'Equilibre Intérieur des Corps Solides Homogenes. Mem. Divers Savans, **4**, 463-562
- Li, Q. Z., & et.al. (2007) X-ray Diffraction Patterns of Graphite and Turbostratic Carbon. Carbon, **45**(8), 1686–1695.
- Macdonald, D. M. (1971) The Development of Prow and Wedge Type Junctions in Shrink-Fitted Torsion Joints. Wear, **18**(1), 41–50.
- McMillan, M., Booker, J. D. & Smith. D. J. (2013) Simulation of Interference Fitted Joint Strength as Used in Hot Rolling Work Rolls. In: Dynamic Behavior of Materials, Volume 1, Chalivendra, Vijay; Song, Bo; Casem, Daniel (Eds.), SEM/Springer, 319-326.
- Pirling, T., Bruno, G., & Withers, P. J. (2006) SALSA - A New Instrument for Strain Imaging in Engineering Materials and Components. Materials Science and Engineering: A, **437**(1), 139–144.
- Timoshenko, S. (1970) Strength of Materials Part II: Advanced Theory and Problems (3<sup>rd</sup> Edition), Van Nostrand Reinhold Company, New York.
- Tipler, P. A. & Mosca, G. P. (2004) Physics For Scientists and Engineers - Extended Edition, Fifth Edit. Freeman, New York.